Available online at www.sciencedirect.com
SCIENCE DIRECT®
Acta Materialia 53 (2005) 1407–1413
Acta MATERIALIA
www.actamat-journals.com

Immobilization of metal-containing nanoparticles on the surface of polytetrafluoroethylene nanogranules

S.P. Gubin [a], G.Yu. Yurkov [a,*], M.S. Korobov [a], Yu.A. Koksharov [b], A.V. Kozinkin [c], I.V. Pirog [c], S.V. Zubkov [c], V.V. Kitaev [c], D.A. Sarichev [c], V.M. Bouznik [d], A.K. Tsvetnikov [e]

[a] *Laboratory of Nanomaterials Chemistry, N.S. Kurnakov Institute of General and Inorganic Chemistry, Russian Academy of Sciences, Leninsky prospect 31, Moscow 119991, Russia*
[b] *Faculty of Physics, Moscow State University, Vorobievy Gory 2, Moscow 117234, Russia*
[c] *Institute of Physics, Rostov State University, pr. Stachki 194, Rostov-on-Don 344090, Russia*
[d] *Boreskov Institute of Catalysis, Siberian Division, Russian Academy of Sciences, pr. Akademika Lavrent'eva 5, Novosibirsk 630090, Russia*
[e] *Institute of Chemistry, Far East Division, Russian Academy of Sciences, pr. Stoletiya Vladivostoka 159, Vladivostok 690022, Russia*

Received 19 November 2004; accepted 24 November 2004
Available online 24 December 2004

Abstract

Metal-containing (Fe, Co, Ni, Cu and Pd) nanoparticles have been synthesized and immobilized on the surface of polytetrafluoroethylene nanogranules 150–500 nm in size. X-ray diffraction, transmission electron microscopy, X-ray emission, Mössbauer spectroscopy and EXAFS results demonstrate that the nanoparticles (3.5–6.5 nm) have a complex structure, are isolated from one another and are strongly bonded to the surface of the nanogranules.

Keywords: Nanomaterials; Stabilized nanoparticles; Polymer matrices; Nanoparticle properties

1. Introduction

The great interest in nanostructured materials is motivated by their fascinating magnetic, optical and chemical properties, which depend strongly on the size, composition and structure of their constituents. Particular attention has focused on monodisperse particles several nanometres in size. In many cases, such particles are needed in the form of dry, redispersible powders. A major technological problem is spontaneous aggregation of nanoparticles. One possible solution to this problem is to use supports interacting with nanoparticles.

In the context of nanomaterials engineering [1], considerable attention has been paid in the past few years to nanoparticles supported on the surfaces of various nanocapsules: carbon [4], TiO_2 [2] and mesoporous SiO_2 spheres [3]. As a rule, there is strong interaction between supports and nanoparticles, which prevents the latter from aggregating. This approach has been commonly applied to nanocapsules larger than 100 nm in diameter, which have a significant chemical affinity for nanoparticles. A very promising approach to creating nanomaterials with optimized physical and chemical (catalytic) properties is deposition on semiconductor nanogranules.

Many organic polymers have also been used in various nanoparticle surface engineering approaches [5]. Most of the research effort has been concentrated on nanoparticulate core/polymer shell systems with SiO_2,

* Corresponding author. Tel.: +7 95 954 7136; fax: +7 95 954 1279.
E-mail addresses: gy-yurkov@yandex.ru, iourkov76@yandex.ru (G.Yu. Yurkov).

1359-6454/$30.00
doi:10.1016/j.actamat.2004.11.033

Au and other cores. There has been less work on polymer core/nanoparticulate shell systems, clearly because most polymers are difficult to prepare in the form of nanodispersions. Therefore, the development of new techniques for stabilizing metallic nanoparticles on the surface of polymer cores is a challenging problem. In this work, polytetrafluoroethylene nanogranules (PTFENGs) 150–500 nm in diameter are used to stabilize various metal-containing nanoparticles (MCNPs). The nanogranules were fabricated by the thermal gas-dynamic method, suitable for commercial-scale production of nanopowders.

Here, we report a simple and efficient chemical process, using metal-containing compounds as precursors, for coating PTFENGs with nominally monodisperse MCNPs. The nanoparticles are examined by X-ray diffraction (XRD), transmission electron microscopy (TEM), EXAFS spectroscopy, X-ray emission and Mössbauer spectroscopy. This work has been motivated by potential applications of PTFENG/MCNP systems.

2. Experimental procedures

2.1. Sample preparation

PTFENG/MCNP core–shell systems (where the core is PTFENG, and the shell is MCNP) were prepared via thermal decomposition of metal-containing precursors on the surface of PTFENGs in mineral oil, as described previously [6]. We used commercially available high-quality PTFENGs [7]. Although the nanogranules were nominally pure, their IR spectrum showed a weak feature at 1780 cm^{-1}, due to C=O vibrations. All preparation steps were carried out by standard techniques in argon. The precursors and solvents (Aldrich Chemical and Acros Organics) were used as-purchased, with no additional purification. The mineral oil was purified in concentrated H_2SO_4, washed, dried and degassed at 250 °C.

To produce MCNPs from MRn (M = Co, Fe, Cu, Ni, Pd; R = CO, HCOO, CH_3COO) precursors, we used well-documented thermal (or photoinduced) decomposition processes. These processes are well suited to our purposes since their by-products are volatile and, hence, can be removed easily at high temperatures. Previously, similar procedures were used to embed nanoparticles in polymer matrices [6].

The sample preparation procedure is schematically illustrated in Fig. 1. We found that, at PTFENG sizes from 100 to 500 nm, a fluidized bed of nanogranules was formed over the surface of heated oil. This behaviour of nanogranules was used to immobilize MCNPs.

The process conditions were adjusted so that the new phase was only formed on the PTFENG surface and not in the oil: the nanogranules offered nucleation sites for nanoparticle formation. In the course of deposition, the nanogranules became progressively heavier, and some of them left the fluidized bed and settled in the oil. As a result, the MCNPs on their surfaces stopped growing.

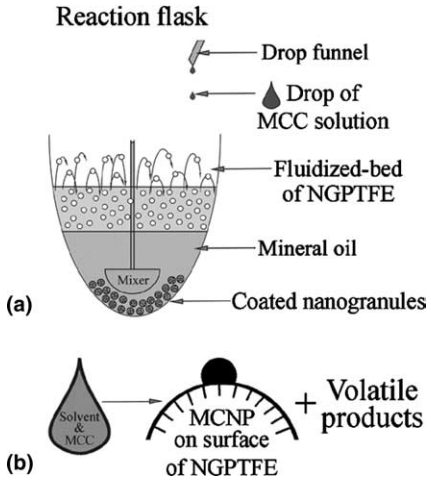

Fig. 1. (a) Schematic of PTFENG metallization; (b) formation of nanoparticles on the PTFENG surface in the course of metallization.

The typical procedure for fabricating PTFENG/MCNP core–shell systems was as follows. An aqueous (organic) solution of a metal-containing precursor was added dropwise to a vigorously stirred suspension of PTFENGs in oil heated to 250–300 °C. The mixture was then held at temperature for 0.5 h for the reaction to reach completion. After cooling to room temperature, the resultant dark precipitate was isolated by decantation and filtration and then washed with an organic solvent until free of oil.

3. Results and discussion

3.1. Characterization of the samples

The metal content of the samples was determined by elemental analysis. A typical powder XRD pattern of the PTFENG/MCNP (M = Cu) material is displayed in Fig. 2. It shows diffraction lines characteristic of copper metal, without peaks attributable to copper oxides or other copper-based phases. In the case of other metals, we observed a more complicated picture.

TEM images were taken on a JEOL JEM-100B at an accelerating voltage of 100 kV. TEM specimens were prepared by placing a drop of an alcoholic suspension of nanogranules on a carbon-coated copper grid. Fig. 3 shows a representative TEM image of as-prepared PTFENG/MCNPs. The deposition of nanoparticles markedly changes the surface morphology: there are numerous dark islands on the (initially smooth) nanogranule surface, which consist of MCNPs. As seen in

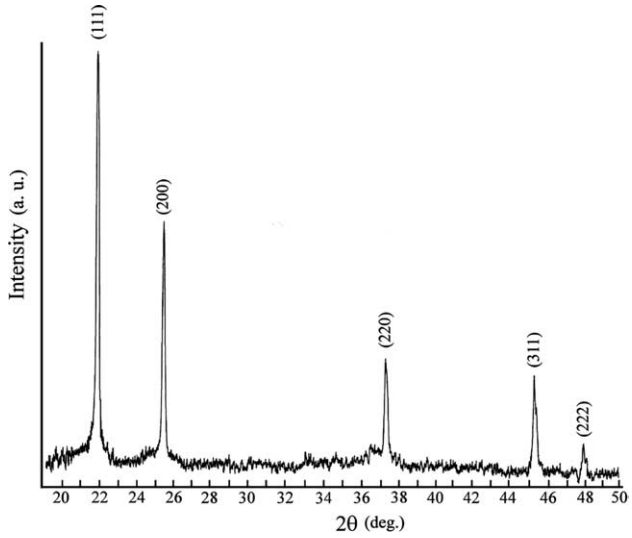

Fig. 2. XRD pattern of PTFENG/Cu; the peaks from PTFE are omitted.

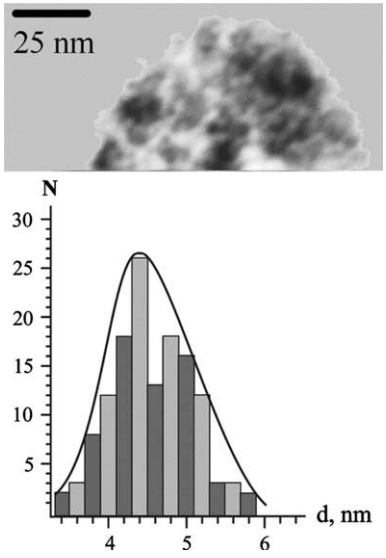

Fig. 3. TEM micrograph of Fe-containing nanoparticles ($d \approx 5.0 \pm 0.5$ nm) on the PTFENG surface and the corresponding particle size distribution.

Fig. 3, MCNPs are distributed rather evenly throughout the PTFENG surface. We find that all the nanogranules in our samples are covered with nearly monodisperse MCNPs. From the TEM image in Fig. 3, the average size of the MCNPs [γ-Fe_2O_3 prepared from $Fe(CH_3COO)_3$] was determined to be ≈5 nm, with a narrow size distribution. The size distribution was assessed by examining more than 130 nanoparticles. The average sizes of Co- and Pd-containing nanoparticles were 3.5 and 7.5 nm, respectively. Although the number of MCNPs surrounding each PTFENG varied from sample to sample, we were able to control the total amount of the deposited metal per nanogranule by varying the precursor concentration in the solution.

Additional information about the composition and structure of MCNPs can be gained from EXAFS, X-ray emission and Mössbauer spectra. Fe $K\beta_5$ X-ray emission spectra were measured as described elsewhere [8]. EXAFS spectra above the Fe K edge were recorded in transmission on the EXAFS spectrometer at the Siberian Synchrotron Radiation Centre, with the storage ring operating at a beam energy of 2 GeV and current of 80 mA. The X-ray energy was selected by an Si(1 1 1) double-crystal monochromator. The incident and transmitted X-ray intensities were measured with Ar-filled ionization chambers. EXAFS data were analyzed using the UWXAFS code [9]. Mössbauer spectra were recorded with an MC1101E high-speed spectrometer. The gamma source used was chromium-shielded ^{57}Co. Isomer shifts were measured relative to α-Fe. The results were analyzed using the UNIVEM-MS code for Mössbauer data processing.

The 90-K Mössbauer spectrum of a PTFENG/MCNP sample (M = Fe, 4.1 wt%) prepared using $Fe(CO)_5$ is shown in Fig. 4. The spectrum can be decomposed into four sextets and two central doublets. The sextets, with magnetic hyperfine fields Hhyp = 341, 247, 220 and 136 kOe, are attributable to α-Fe and three carbide nanophases, respectively. The α-Fe content evaluated from Mössbauer results is 15%, and that of the carbide phases is 48%. The doublet with a quadrupole splitting QS = 1.069 mm/s and an isomer shift IS = 0.447 mm/s seems to be due to compounds containing trivalent Fe, probably iron oxides. The estimated content of these compounds is 25%. The doublet with QS = 2.903 mm/s and IS = 1.502 mm/s is attributable to compounds containing divalent Fe. TEM micrographs demonstrate that the nanoparticles are isolated from one another and are distributed rather evenly over the PTFENG surface. One would expect that the phase containing divalent Fe (FeF_2) is present in nanoparticle/PTFENG interfacial regions. The number of Fe atoms interacting with each nanogranule is not very large; accordingly, the FeF_2 content is rather low (12%).

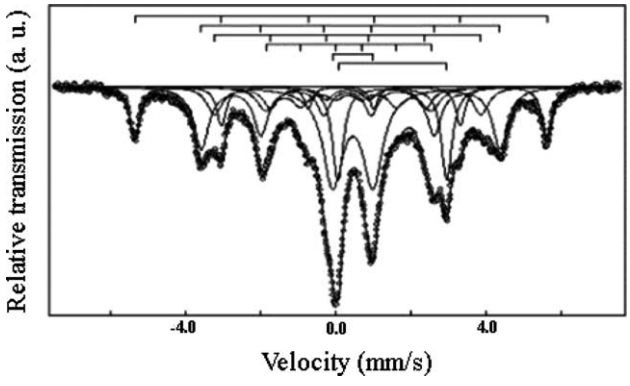

Fig. 4. Mössbauer spectrum of PTFENG/Fe.

3.2. X-ray emission spectra

The Fe $K\beta_5$ spectrum of the PTFENG/MCNP (4.1 wt% Fe) sample shows three prominent components, labelled A, B and C. The parameters of the spectrum are listed in Table 1 in comparison with those for standard Fe compounds. As follows from its energy position, component A, corresponding to the maximum in the spectra of α-Fe and Fe_3C, arises from the interaction of Fe valence p-orbitals with 3d-orbitals of nearest neighbour Fe atoms (so-called metal–metal bonds) [8,12]. Components B and C originate from the interaction of Fe valence p-orbitals with C 2p- and 2s-orbitals, respectively. The Fe $K\beta_5$ spectrum of the sample contains the same prominent features as the spectrum of Fe_3C [8].

In addition, there are features D and E on the low-energy side of the major peak (15 and 22 eV, respectively). These features are due to the interaction between the Fe valence p-orbitals and the O and F 2s-orbitals, and their energy positions agree with those in earlier studies [8,10–12].

On the high-energy side of component A, there is a satellite (A′) which is characteristic of iron oxides and fluorides but is missing in the X-ray emission spectrum of Fe [8,12]. Thus, the Fe $K\beta_5$ spectrum indicates that the nanoparticles studied here contain several Fe compounds and that the Fe atoms in the PTFENG/MCNP system may be co-ordinated to carbon, oxygen and fluorine atoms.

To assess the phase composition of the nanoparticles, the Fe $K\beta_5$ spectrum was decomposed into components arising from α-Fe, Fe_3C, Fe_2C_5, Fe_2O_3 and FeF_2. It was found that the net content of the carbide phases was about 45%, and those of α-Fe, Fe_2O_3 and FeF_2 were about 12%, 25% and 18%, respectively, in good agreement with Mössbauer results.

3.3. EXAFS

The normalized EXAFS spectrum of the Fe K edge for the PTFENG/MCNP (4.1 wt% Fe) sample prepared using $Fe(CO)_5$ shows a narrow strong peak at the Fe K edge, which attests to the presence of low Z atoms in the nearest neighbour environment of Fe. The Fourier transforms of the k^1- and k^3-weighted spectra were computed over the range of photoelectron wave numbers $k = 3.1–12.4$ Å^{-1} (Fig. 5).

The first prominent peak in Fig. 5(a) ($r \sim 1.5$ Å) corresponds to the nearest neighbours of the Fe atoms. The asymmetry of this peak indicates that the chemical environment of Fe has a complicated composition. The mean nearest neighbour distance is ~2 Å (after phase correction), characteristic of bonds between Fe and low Z atoms (C, O, F). The k^3-weighted Fourier transform, in which the relative contribution from high Z atoms is more important [13], reveals a prominent peak at $r \sim 2.2$ Å, corresponding to Fe–Fe interaction (Fig. 5(b)). The fact that this peak only emerges in the k^3-weighted Fourier transform suggests that the percentage of metallic Fe in the nanoparticles is rather small. The peaks at $r \sim 3.5$ and 4.5 Å are characteristic of the bcc structure of α-Fe and also indicate that the nanoparticles contain only a small amount of Fe metal. To determine the structural parameters of the first- and second-neighbour environments, we carried out non-linear fitting [9] of the experimental data by spectra simulated with the use of FEFF7 [14]. Since the first and second peaks in Fig. 5(b) overlap, a two-step fitting procedure was used. First, the structural characteristics of the second neighbours, corresponding to Fe–Fe bonds, were evaluated. To reduce the contribution from the low Z atoms to the second peak, fitting was carried out in the ranges $k = 4.9–13.3$ Å^{-1} and $r = 1.8–2.8$ Å. The Fe–Fe co-ordination number in the nanoparticles was found to be smaller than that in bulk α-Fe, indicating that the crystal structure of the nanoparticles was distorted on account of the small size of the Fe core.

Next, the composition and structural parameters of the nearest neighbour environment were refined. Fitting was carried out in the ranges $r = 1.0–2.8$ Å and $k = 3.1–12.4$ Å^{-1}. Attempts to represent the co-ordination of Fe by a single model (only iron carbide or fluoride or oxide) were unsuccessful. In view of this, we tried phase mixtures and evaluated the structural parameters of the nearest neighbour environment using the Fe–C, Fe–O and Fe–F backscattering paths known

Table 1
The bands in Fe $K\beta_5$-spectra of the sample PTFENG/MCNP (M = Fe; 4.1%wt, obtained from $Fe(CO)_5$) and for comparison the data for standard compounds

Compound	Fe $K\beta_5$-spectra components, eV				
	A	B	C	D	E
Sample	7108.0	7106.4	7109.2	7091.1	7084.5
α-Fe	7108.0	–	–	–	–
Fe_3C	7108.0	7106.3	7109.1	–	–
Fe_2O_3	–	7106.5	–	7091.2	–
FeF_2	–	7105.8	–	–	7084.4

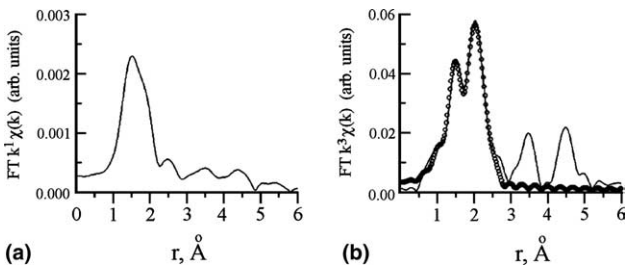

Fig. 5. Fourier transforms of the (a) k^1- and (b) k^3-weighted spectra of PTFENG/MCNP.

for bulk Fe_2C_5, γ-Fe_2O_3 and FeF_2. As input parameters, we took the contents of these phases inferred from X-ray emission and Mössbauer spectroscopy data. The contributions from different phases were added using mixing parameters. In this way, the contributions of the iron carbides, iron fluoride and iron oxides to the first neighbour co-ordination were evaluated to be 50%, 20% and 30%, respectively, with an estimated uncertainty of about 1%. The best fit curve is shown in Fig. 5(b) together with the Fourier transform of the experimental spectrum. The EXAFS results agree well with the phase composition inferred from Mössbauer data.

Thus, some of the Fe atoms are co-ordinated by carbon atoms, and some, by fluorine and oxygen atoms. The major phases in the nanoparticles are Fe_3C and Fe_2C_5 (~47%), the Fe metal content is estimated at 16%, and the γ-Fe_2O_3 and FeF_2 contents are about 26% and 11%, respectively. Fig. 6 shows the structural model of nanoparticles on the PTFENG surface inferred from these results. The model ensures the best agreement with experimental data and fits well with EXAFS, X-ray emission and Mössbauer spectroscopy data. The possibility of PTFE defluorination by metallic nanoparticles was examined earlier [15].

3.4. Magnetic properties

The Co-containing nanoparticles with an average diameter of ≈3.5 nm (Fig. 7) in the sample with a Co content of about 4 wt% were found to possess interesting magnetic properties. Fig. 8 shows the variation of the magnetic moment M during zero-field cooling (ZFC). Above ≈25 K, the temperature variation of M is typical of ZFC experiments with single-domain magnetic nanoparticles: the magnetic moment increases with temperature and reaches a maximum at an average blocking temperature $\langle T_B \rangle \approx 270$ K. At room temperature, the sample has a rather low magnetization, $M \approx 9$ emu/g Co (at 6 kOe), which is markedly lower than the bulk value (160 emu/g Co), and a significant coercive field (≈600 Oe). The magnetic anisotropy of the nanoparticles was estimated as $K_V \approx 30 k_B T / V \approx 6 \times 10^5$ erg/cm^3, which is comparable to the bulk value (10^6 erg/cm^3). In our recent work [16], cobalt

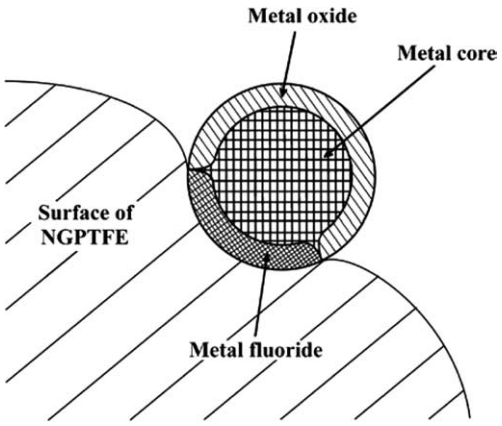

Fig. 6. Structural model of metal-containing nanoparticles on the PTFENG surface.

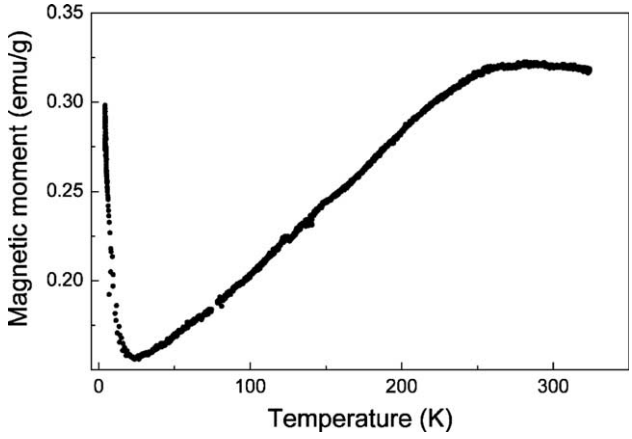

Fig. 8. Magnetic moment of the sample containing 4% Co in a zero-field cooling experiment; measurements in a field of 2.25 kOe.

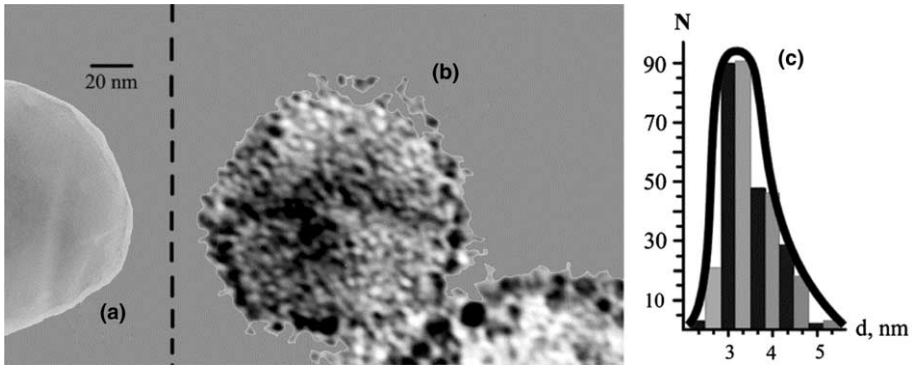

Fig. 7. TEM micrographs of (a) a PTFENG ($d \sim 150$ nm) and (b) Co-containing nanoparticles ($d = 3.5 \pm 0.5$ nm) on the PTFENG surface; (c) nanoparticle size distribution.

nanoparticles of nearly the same average diameter (4 nm), dispersed in a polyethylene matrix have shown markedly higher values: $\langle T_B \rangle \approx 600$ K and $K_V \approx 6 \times 10^7$ erg/cm^3.

Since the particle concentration in our samples is low, we neglect the magnetic interactions between the particles and take into account only the surface and finite-size effects. The surprisingly high magnetic anisotropy of nanoparticles is commonly interpreted in terms of surface effects. However, a significant reduction in K_V may result not only from interfacial conditions, which are very specific in this work, but also from the complex chemical composition of the nanoparticles. Indeed, below 25 K the magnetic moment shows an unusually sharp increase (Fig. 8). It is not inconceivable that this effect is due to very small nanoparticles, which behave as paramagnets even at very low temperatures. We however failed to discern such small nanoparticles in TEM images of our samples. Another possible reason is that the nanoparticles contain CoF_2. As found by Lines [17], the perpendicular magnetic susceptibility of bulk CoF_2 grows significantly below the Néel temperature (≈38 K). Since the magnetic transition temperature in nanoparticulate systems tends to be lower than that in their bulk counterparts, it is possible that the low-temperature anomaly in our samples results from the presence of the antiferromagnetic phase CoF_2, as supported by the low value of magnetization.

The complex broadening pattern in the EPR spectrum also suggests that the nanoparticles consist of several phases. Fig. 9 shows the room-temperature and 77-K EPR spectra of the sample containing Co-based nanoparticles. The shape of the resonance line is seen to be temperature-dependent: with decreasing temperature, the spectrum broadens and shifts to lower fields (Fig. 9). Moreover, the weak feature near $g = 2.00$ disappears on cooling to 77 K. At room temperature, there are at least three distinct lines, near $g = 2.0$ and 2.5 and at very low fields. The signals with g-factors differing from 2.00 are likely to result from CoF_2.

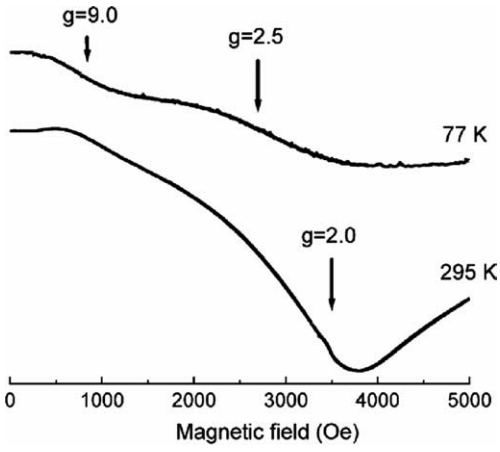

Fig. 9. Room-temperature and 77-K EPR spectra of the sample containing 4 wt% Co.

Thus, our magnetic and EPR data suggest that the nanoparticles in the sample containing 4 wt% Co have a complex internal structure, including, probably, a metallic cobalt core and a surface layer of CoF_2 and/or CoO.

Preliminary results on the catalytic activity of PTFENG/Pd-NPs were obtained using phenylacetylene hydrogenation as a test reaction. The PTFENG/Pd sample was found to exhibit catalytic activity comparable to that of conventional Pd catalysts. Systematic studies are needed to characterize this unique catalyst, consisting of metallic nanoparticles immobilized on the surface of PTFENGs, a novel type of support.

The nanomaterials studied in this work are potentially attractive for a number of other applications. We believe that PTFENGs covered with magnetic nanoparticles are of great interest for technological applications ranging from magnetic recording to biodiagnostics and therapy. They are also candidate materials for permanent magnets: melting PTFENG/Fe-NP powder at ~320 °C under a layer of oil, we have for the first time obtained magnetic PTFE [7]. It is interesting to extend the approach described here to other magnetic, semiconducting, dielectric and ferroelectric nanoparticles in order to stabilize them on the surface of nanogranules. Further studies of PTFENGs as supports for such nanoparticles are under way in our laboratory.

4. Summary

In summary, we have developed a novel procedure for the immobilization of nanoparticles which offers the possibility of controlling the properties and stability of various nanoparticles. The PTFENGs and MCNPs have been examined by TEM. The results indicate that the nanoparticle size is in the range 3.5–7.5 nm. We have also analysed in detail the composition of the nanoparticles. The core–shell structure of the PTFENG/MCNP samples has been confirmed by TEM, EXAFS, Mössbauer and X-ray emission results.

Acknowledgements

We thank Prof. T.A. Stromnova for informing us of her preliminary results on the catalytic activity of the Pd-containing sample. This work was supported by the Russian Foundation for Basic Research (Grant Nos. 02-03-32435, 02-03-32321, 04-03-32090, 04-03-32311, 04-03-32597), the International Science and Technology Centre (Project no. 1991), the Russian Science Support Foundation and the Russian Academy of Sciences (RAS) (programmes: Fundamental Issues in the Physics and Chemistry of Nanosystems and

Nanomaterials, and Controlled Synthesis of Inorganic Substances with Tailored Properties, and Fabrication of Functional Materials) and the Siberian Division of RAS (Project no. 18.07).

References

[1] Moriarty P. Rep Prog Phys 2001;64:297.
[2] Pastoriza-Santos I, Koktysh DS, Mamedov AA, Giersig M, Kotov NA, Liz-Marzan LM. Langmuir 2000;16:2731.
[3] Sadtler B, Wei A. Chem Commun 2002:1604.
[4] Lau KT, Hui D. Composites Part B 2002;33:263.
[5] Jeszka JK, Tracz A, Wostek D, Boiteux G, Kryszewski M. Synth Met 2000;109:165.
[6] Gubin SP. Colloids Surf A 2002;202:155.
[7] Gubin SP, Korobov MS, Yurkov GYu, Tsvetnikov AK, Buznik VM. Dokl Chem 2003;388:44.
[8] Kozinkin AV, Sever OV, Gubin SP, Shuvaev AT, Dubovzev IA. Neorg Mater 1994;30:678.
[9] Stern EA, Newville M, Ravel B, Haskel D, Yacoby Y. Physica B 1995;208 and 209:117.
[10] Nefedov VI, Kurmaev EZ, Porai-Koshits MA. Zh Strukt Khim 1972;13:637.
[11] Nefedov VI. Itogi Nauki Tekh 1975;3:177.
[12] Kozinkin AV, Vlasenko VG, Gubin SP, Shuvaev AT, Dubovzev IA. Neorg Mater 1996;32:422.
[13] Kochubey DI, Babanov YuA, Zamaraev KI, Vedrinsky RV, Kraizman VL, Kulipanov GN, et al. X-ray spectroscopy technique for structure investigation of amorphous compounds: EXAFS spectroscopy. Moscow: Nauka; 1988. p. 303.
[14] Zabinski SI, Rehr JJ, Ancudinov A, Albers RC, Eller MJ. Phys Rev B 1995;52:2995.
[15] Kosobudsky ID, Kashkina LV, Gubin SP, Petrakovsky GA, Piskorskii VP, Svirskaya NM. Vysokomol Soedin 1985;4:669.
[16] Gubin SP, Spichkin YuI, Koksharov YuA, Yurkov GYu, Kozinkin AV, Nedoseikina TI, et al. J Magn Magn Mater 2003;265:234.
[17] Lines ME. Phys Rev 1965;137:982.